B. Manchon,* G. Segantini, N. Baboux, P. Rojo Romeo, R. Barhoumi, I. C. Infante, F. Alibart, D. Drouin, B. Vilquin, D. Deleruyelle 2100585

Insertion of an Ultrathin Interfacial Aluminum Layer for the Realization of a $Hf_{0.5}Zr_{0.5}O_2$ Ferroelectric Tunnel Junction

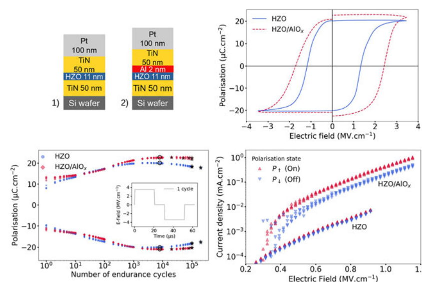

Metal–insulator–ferroelectric–metal structure has recently been brought to the spotlight as a way to make Ferroelectric Tunnel Junction without the need for ultrathin ferroelectric layer. Herein, the first use of an ultrathin Al layer is presented for the fabrication of an MFIM HZO–based FTJ through the scavenging of oxygen from the HZO during annealing. Herein, a small increase of remanant polarization, a large increase in conductivity and an On/Off ratio of up to 3.7, is reported.

Q1

UNCORRECTED PROOF

Insertion of an Ultrathin Interfacial Aluminum Layer for the Realization of a $Hf_{0.5}Zr_{0.5}O_2$ Ferroelectric Tunnel Junction

Q2 *Benoît Manchon*,* *Greta Segantini*, *Nicolas Baboux*, *Pedro Rojo Romeo*, *Rabei Barhoumi*, *Ingrid C. Infante*, *Fabien Alibart*, *Dominique Drouin*, *Bertrand Vilquin*, and *Damien Deleruyelle*

Herein, the effect of a 2 nm thin aluminum layer inserted between the ferroelectric layer and the top electrode in a TiN/$Hf_{0.5}Zr_{0.5}O_2$/TiN stack deposited by reactive magnetron sputtering is investigated. The oxidation of the interfacial layer during annealing due to scavenging of the $Hf_{0.5}Zr_{0.5}O_2$ impacts both the ferroelectric properties and the electrical conductivity of the junction. It is shown that the overall conductivity of the junction is boosted 20 folds while the resistance ratio between the positive and negative polarization states is increased from 1.3 up to 3.7. Through a systematic analysis of programming conditions, pulse duration, and height, we show that both the remanent polarization and On/Off current ratio can be enhanced at the expanse of the endurance leading to a trade-off.

1. Introduction

The unique properties of ferroelectric materials have been exploited to date in numerous integrated devices such as Ferroelectric Random Access Memories, Ferroelectric Field Effect Transistors, Negative Capacitance Field Effect Transistors, and Ferroelectric Tunnel Junctions (FTJs).[1] The discovery of ferroelectricity in Si-doped hafnium oxide in 2011[2] gave a significant boost to research on the topic. Although other successful dopants have been found,[3] the solid solution $Hf_{0.5}Zr_{0.5}O_2$ (HZO) has attracted a lot of interest.[4] Hafnia-based thin films present the double advantage of already being widely used in the semiconductor industry and of having a significantly lower crystallization temperature as compared to perovskite ferroelectrics, with reported values as low as 300 °C,[5] allowing therefore full compatibility with both front-end and back-end of line integration.

FTJs are tri-layer structures in which two electrodes consisting either of metals or highly doped semiconductors sandwich a thin ferroelectric layer. The internal field of the ferroelectric layer attracts or repels charges at the interfaces with the electrodes. Due to differences in screening lengths and permittivities of the electrode materials, the polarization direction induces a modulation of the potential barrier. The polarization state can then be probed through the measurement of tunneling currents. Although ferroelectric HZO has been demonstrated down to 1 nm thick layers,[6] scaling HZO thickness down to a few nanometers while maintaining good ferroelectric properties remains a real fabrication challenge.[7] The resistance variation in an ideal FTJ is only due to direct tunneling; however, real FTJs are complex devices where several competing charge transport mechanisms can occur

B. Manchon, N. Baboux, I. C. Infante, D. Deleruyelle
INSA Lyon
ECL
CNRS
UCBL
CPE Lyon
INL
UMR5270
Univ Lyon
69621 Villeurbanne, France
E-mail: benoit.manchon@insa-lyon.fr

B. Manchon, D. Drouin
Institut Interdisciplinaire d'Innovation Technologique (3IT)
Université de Sherbrooke
Sherbrooke, Québec, Canada

B. Manchon, D. Drouin
Laboratoire Nanotechnologies Nanosystèmes (LN2) CNRS UMI-3463 Q3
Québec, Canada Q4

G. Segantini, P. Rojo Romeo, R. Barhoumi, B. Vilquin
ECL
INSA Lyon
CNRS
UCBL
CPE Lyon
INL
UMR5270
Univ Lyon
69130 Ecully, France

F. Alibart
Institute of Electronics
Microelectronics and Nanotechnology (IEMN)
Université de Lille
Villeneuve d'Ascq, France

Q-license DOI: 10.1002/pssr.202100585

UNCORRECTED PROOF

© 2022 Wiley-VCH GmbH

simultaneously. In addition, more than one physical mechanism can be involved in the resistance modulation. In this work, we will define FTJs as ferroelectric devices, which exhibit a change in their electrical resistance depending on polarization direction. Therefore, the term "tunneling currents," in its broad sense, will refer to all charge transport modes across a dielectric (such as direct tunneling, Fowler–Nordheim tunneling, thermionic emission, and so on) rather than just direct tunneling. Recently, a slightly different structure has been brought in the spotlight. Theorized by Meyer et al.,[8] the addition of an ultrathin dielectric layer, resulting in a metal/ferroelectric/insulator/metal (MFIM) structure, enables conductance modulation with thicker ferroelectric layers. The inserted dielectric layer plays the role of tunneling barrier while the ferroelectric layer acts as a polarization switch. In this context, several devices exploiting Al_2O_3 and TiO_2 interfacial layers have recently been reported in the literature.[9–12]

An important parameter in the stabilization of the ferroelectric phase in doped HfO_2 is the oxygen content. It has mainly been studied in atomic layer deposition processes and the results indicate that the formation of the orthorhombic and tetragonal phases can be promoted by oxygen vacancies.[13] In this work, the affinity of Al for oxygen atom was exploited to combine the fabrication of an MFIM junction with the generation of oxygen vacancies in HZO layer to promote the ferroeletric phase. A set of twin samples was fabricated to study the influence of an ultrathin interfacial Al layer. Their structure is depicted in **Figure 1**. A symmetrical TiN/HZO/TiN stack serves as reference to the second sample which had a 2 nm thick layer of Al inserted at the top electrode interface: TiN/HZO/Al/TiN. The ferroelectric HZO layer is 11 nm thick for both samples. Although symmetrical electrodes cannot, in theory, produce an On/Off ratio, symmetrical FTJs have been demonstrated due to interfacial differences between the top and bottom contact (interface reconstruction, exposure to air, and so on).[14] It is theorized that the Al layer formed a dielectric AlO_x layer during the annealing step by scavenging oxygen atoms from the HZO layer. We report the first use of an oxygen scavenging ultrathin Al layer for the fabrication of an HZO-based FTJ. The aim was to obtain the same effect as an interfacial layer of Al_2O_3 to increase On/Off ratio of FTJ devices while also generating oxygen vacancies, which play an important yet not fully understood role in the stabilization of the ferroelectric orthorhombic phase.

2. Results and Discussion

The glancing incidence X-ray diffraction (GI-XRD) patterns shown in Figure 1a indicate the poly-crystalline nature of the HZO layers. The position of the peak at $2\theta \approx 30.5°$ is consistent with the theoretical value of the orthorhombic/tetragonal phase for the (111) plane and confirms the presence of the ferroelectric phase. The monoclinic (11–1) and (111) peaks at $2\theta \approx 28.4°$ and $2\theta \approx 31.6°$, respectively, are also detected. Using pseudo-Voigt functions that account for Cu Kα1 and Kα2 radiations to fit the data shown in Figure 1b, an analysis of the integrated areas corresponding to the orthorhombic and monoclinic peaks was performed. The presence of orthorhombic phase in the sample with the Al layer was found to be higher by a factor 3 when compared to the one without Al, suggesting that the Al layer helped the formation of the ferroelectric phase. This is consistent with the idea of oxygen vacancies helping the formation of the orthorhombic phase. However, these statements are mitigated by the fact that the diffraction signal originates both from HZO capped and uncapped by the top electrode. The importance of tensile strain provided by top electrode capping in the stabilization of the orthorhombic phase is well documented.[15,16] HZO not covered by the top electrode is unlikely to form the orthorhombic phase and the monoclinic phase is therefore overevaluated. Here, the surface ratio of HZO covered by the top electrode is about 50%. In addition, the overlap of the orthorhombic and tetragonal peaks makes the quantitative analysis of the two phases rather difficult.

The relative permittivity (ε_r) against voltage plots obtained from capacitance measurements plotted on Figure 1c exhibits the characteristic butterfly shape of ferroelectric capacitors. The extracted relative permittivity of the HZO/AlO_x stack is lower than that of the reference as would be expected with the addition of a second dielectric layer. This finding is in favor of our assumption that the deposited Al has been oxidized during annealing. To further support this statement, the theoretical permittivity versus voltage curve of the HZO/AlO_x sample, $\varepsilon_r^{computed}$,

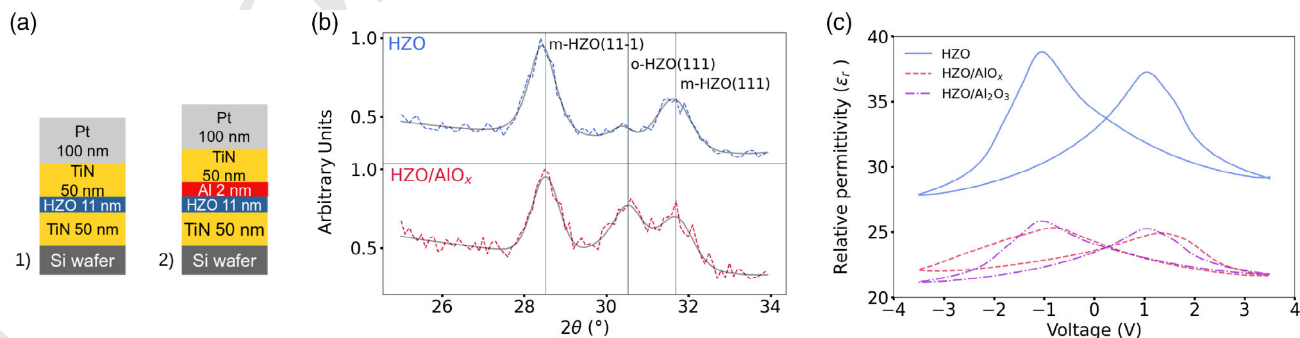

Figure 1. a) Structure of the two samples studied in this work, not to scale. Typical device diameters studied are 20, 50, and 100 µm. b) GIXRD diffraction pattern corresponding to each sample. The fits were obtained using pseudo-Voigt functions accounting for the Cu Kα1 and Kα2 radiations. c) Relative permittivity obtained from capacitance versus voltage sweeps taken between ±3.5 V on both samples. The relative permittivity of the $Hf_{0.5}Zr_{0.5}O_2$ (HZO)/AlO_x corresponds to the average of the double layer. The HZO/Al_2O_3 curve is computed from the reference HZO by adding a theoretical 2 nm layer with a relative permittivity of 9.1 corresponding to Al_2O_3.

© 2022 Wiley-VCH GmbH

1 was computed from the permittivity curve of the HZO reference 2 sample, ε_r^{HZO} with thickness $d_1 = 11$ nm, by adding an interfacial 3 series capacitance of thickness $d_2 = 2$ nm and relative permittiv- 4 ity ε_r^{IL} using Equation (1). As shown in Figure 1c, a very good 5 match was achieved using $\varepsilon_r^{IL} \approx 9.1$, a value fully consistent with 6 the one of Al_2O_3.[17]

Q8
$$\varepsilon_r^{computed} = \frac{\varepsilon_r^{HZO} \cdot \varepsilon_r^{IL}}{d_2 \cdot \varepsilon_r^{HZO} + d_1 \cdot \varepsilon_r^{IL}} \quad (1)$$

7 The ferroelectric properties were then investigated by cycling 8 the devices and regularly taking positive-up-negative-down 9 (PUND) measurements.[18] The assumption is made that the 10 non-ferroelectric contributions to current are exactly the same 11 in a switching and a non-switching pulse and thus the ferroelec- 12 tric current can be isolated by simple subtraction. The positive 13 and negative remanent polarizations (Pr) for five devices of each 14 sample cycled at equal electric field are plotted **Figure 2**a. 15 The device to device variation of the remanent polarization is 16 very low with an average standard deviation to the mean of less 17 than 1% for the five measurements on each sample. The maxi- 18 mum 2Pr during cycling is slightly increased from 40.5 to 19 43.8 μC cm^{-2} with the addition of the Al interfacial layer. 20 However, the overall endurance is impacted; the reference sam- 21 ple devices all reached at least 1×10^5 cycles while three of the 22 AlO_x devices broke down before, with one as early as 2×10^4.

1 These changes may be attributed to the oxygen vacancies that 2 were introduced, improving remanent polarization by increasing 3 the orthorhombic phase content but precipitating breakdown 4 due to a higher defect density. Oxygen vacancies are thought 5 to help the formation of the orthorhombic phase by reducing 6 the phases relative free energy, reducing the grain size or by play- 7 ing the role of nucleation sites.[19] However, oxygen vacancies are 8 also associated with degraded ferroelectric properties past the sta- 9 bilization process playing a key role in wake up, fatigue, and 10 probably leading to an early dielectric breakdown.[20] Here, it 11 seems a compromise is reached in the AlO_x sample as remanent 12 polarization was improved at the expense of endurance while the 13 wake-up and fatigue behavior remained relatively unchanged. 14 Figure 2c shows the current–voltage characteristics recorded dur- 15 ing the switching pulses of a PUND measurement after 5×10^3 16 cycles while Figure 2b shows the extracted polarization–voltage 17 (P–V) curves after the current from the non-switching pulses was 18 subtracted. The introduction of the interfacial layer has increased 19 the coercive field and created a clear asymmetry in the device's 20 electrical properties. Polarization switching occurs at a higher 21 (absolute) voltage than for the reference while being more 22 gradual. This turns into an increased effective coercive field 23 for both regions (from −1.2 to −1.7 MV cm^{-1} and from 1.3 to 24 2.4 MV cm^{-1}) and a softer slope under negative field in the 25 P–V loop. The increase of the coercive field can be related to 26 the voltage drop through the interfacial dielectric layer making

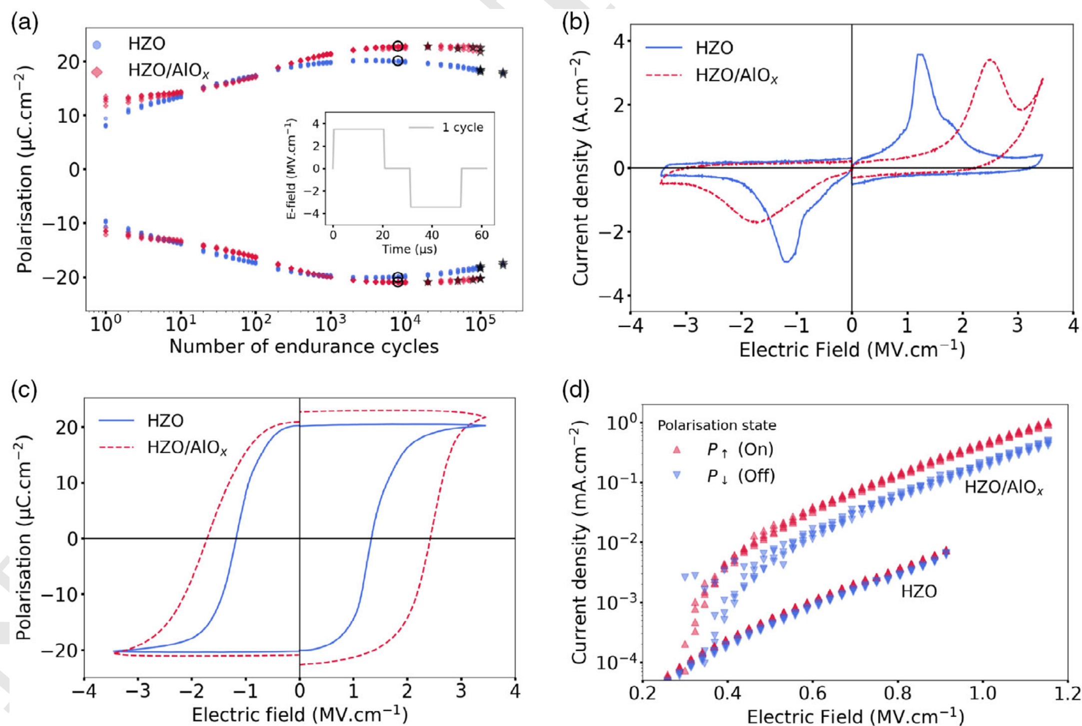

Figure 2. a) Remanent polarization for the reference and the AlO_x sample during cycling until dielectric breakdown. Five of each device were cycled. Stars mark dielectric breakdown. The inset represents one cycle with pulse parameters of ±3.8 V for the reference and 4.5 V for the AlO_x sample ≈3.5 MV cm^{-2}, 500 ns ramps, 20 ms plateau, and 10 ms pause between pulses. b) Current–voltage characteristics of the two samples under applied triangular pulses with 60 µs ramps. These data, as the following polarization curves, are measurements taken after 5×10^3 cycles (data point marked with an empty circle on the endurance graph). c) Polarization versus voltage loops for both samples extracted from the positive-up-negative-down (PUND) measurements. d) Voltage sweeps under the coercive field in the On and Off states for both devices. The measurements were repeated four times.

© 2022 Wiley-VCH GmbH

the voltage requirement higher to reach the coercive field in the HZO layer. One might wonder why Figure 1c does not show the same change in coercive field. It is because the electrical measurement conditions are rather different. The voltage range is not the same and the voltage sweep is quasi-static during the CV measurement as opposed to dynamic for the PUND. Interestingly, the tunneling currents are also drastically increased in the AlO_x sample, most likely due to the number of oxygen vacancies assisting conduction between electrodes.[21] This feature is advantageous for FTJ applications since it allows larger sensing current at low voltages. The increased coercive field may also be beneficial for FTJ applications by allowing a wider range of accessible voltages for read operation without altering the polarization state, therefore giving access to even higher read currents.

Figure 2d shows the plots of current density against electric field taken at low voltages with the polarization facing one or the other electrode for both samples. The measurements were taken 4 times to show repeatability. The On/Off ratio is increased from ≈1.3 to ≈2.4 with the introduction of the Al layer. The small On/Off ratio of the symmetrical device is attributed to a slight interfacial difference due to exposure to air between HZO and top TiN deposition. The maximum current density available for operation in the Off state jumped up from 6.35 to 451 mA cm^{-2}. This is a key parameter for dynamic sensing; for instance, such an increase would allow the reduction of the FTJ diameter from 71 to 8.4 mm to reach a 1 nA sensing current.

The effect of pulse parameters on HZO/AlO_x samples was then investigated by varying pulse widths and heights while monitoring both the remanent polarization and the On/Off current ratio. Both properties increase with pulse width (**Figure 3**a) and height (Figure 3c) at the expense of endurance. There is a trade-off that must be considered when choosing operation parameters. If the endurance appears to follow a more hectic dependency, it is due to the statistical nature of dielectric breakdown. The presence of defects can significantly impact the maximum endurance. The increase in maximum remanent polarization is monotonous for both pulse parameters (**Figure 4**). For best performances, the pulse parameters are 20 ms duration, as it offers the highest On/Off ratio while remaining relatively stable throughout the lifetime of the device, and 3.5 V since it provides the highest endurance. However, for the On/Off ratio, the pulse duration has the biggest influence with not only the value increasing from less than 1.5 to more than 3.5 but also the value becoming increasingly unstable during cycling. Voltage only influences the On/Off ratio up to 3.5 V where a form of saturation is reached. While maximum polarization more than doubles when voltage is increased from 3.5 to 4.5 V, the On/Off ratio remains relatively unchanged. This suggests the origin of the conductivity modulation is not directly dependent on the polarization field or at least not linearly. The oxygen vacancies

Q9

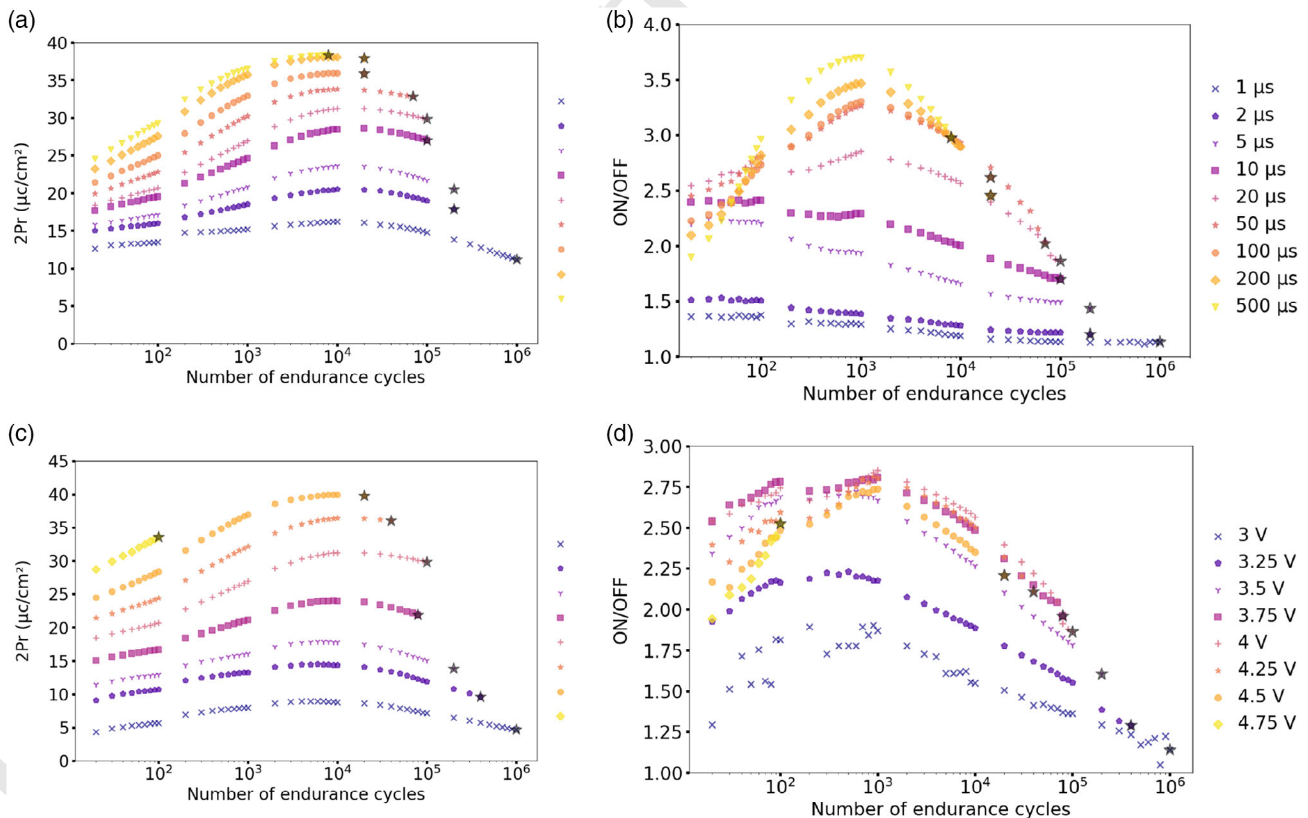

Figure 3. Evolution of remanent polarization a) and On/Off ratios for the AlO_x sample b) during endurance tests carried out with cycling pulse width varying from 1 to 500 μs at 4 V. Evolution of c) polarization and d) On/Off ratio while cycling with pulse heights ranging from 3 to 4.75 V with pulse duration of 20 μs. Stars mark dielectric breakdown.

© 2022 Wiley-VCH GmbH

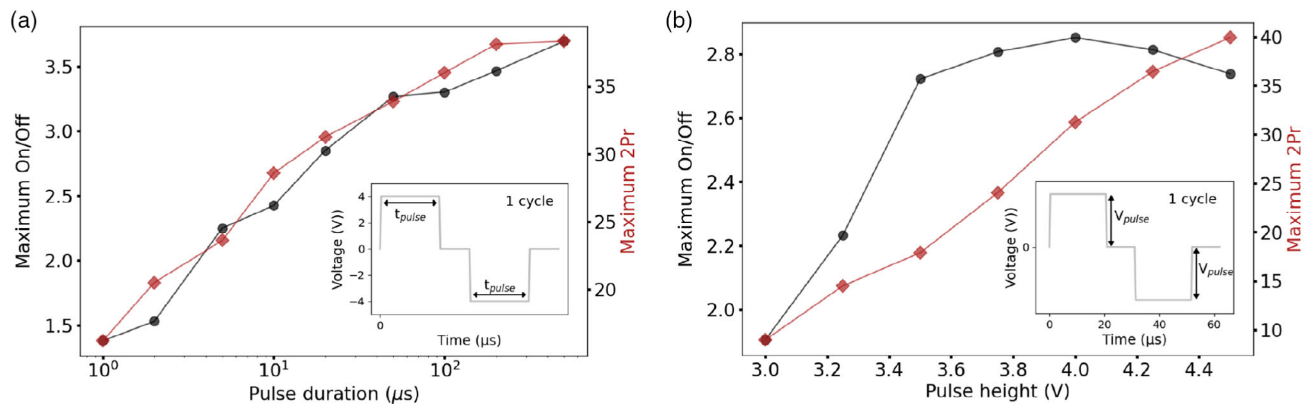

Figure 4. Maximum On/Off current ratios (dots) and remanent polarizations (diamonds) as a function of a) pulse duration and b) height. Insets represent the cycling pulses that were applied with the relevant parameters, as indicated.

migrating under the effect of the applied external field and the ferroelectric polarization are thought to be an important factor at play. We suspect that, similarly to the memristor model presented by Strukov et al.,[22] the oxygen vacancies which are packed at the AlO_x/HZO interface migrate in and out of the ferroelectric layer under the effect of the applied field and of the ferroelectric polarization, lowering and increasing resistivity by creating available states for trap-assisted tunneling. Carrying out current–voltage measurement over an extended temperature range would be helpful to elucidate the prevalence of the different resistance modulation mechanisms and it will be the subject of further investigations.

3. Conclusion

The impact of inserting an ultrathin Al layer in HZO-based FTJ was investigated. With respect to reference devices, it is shown that the insertion of the Al layer leads to an increase of both the remanent polarization and tunneling currents. Oxidation of the Al layer into interfacial AlO_x by scavenging oxygen ions was found to be consistent with CV measurements. It is therefore believed that oxygen vacancies generated through oxidation of the Al layer promoted the formation of the orthorhombic phase of HZO while actively participating to the increase of leakage currents. The On/Off current ratio was improved from 1.3 to up to 3.5 in conjunction with a drastic increase of electrical conductivity, which is beneficial for FTJ operations. Through studying the effect of cycling pulse amplitude and duration, it is shown that both the remanent polarization and On/Off current ratio can be tailored but they are increased at the expense of endurance.

4. Experimental Section

Device Fabrication: The fabrication process of the two samples was thought out to have as little difference between them as possible. A piece of n^+ Si (100) Si wafer was first cleaned using acetone and ethanol followed by a bath in a buffer oxide etching (BOE) solution to remove the native oxide layer. The 50 nm thick TiN bottom electrode was then deposited from a Ti target and a N_2 plasma by reactive magnetron sputtering inside an AC450-sputtering machine by Alliance Concept (all deposition steps were carried out in this equipment). HZO of 11 nm was deposited by nonreactive sputtering of a ceramic $Hf_{0.5}Zr_{0.5}O_2$ target. The piece of Si was then cleaved in halves for the UV lithography step preparing for the liftoff. On one half, 50 nm of TiN and 100 nm of Pt thick circular pads were added as top electrode. The purpose of the Pt was to improve the electrical contact with the metallic tips used for electrical characterization. An ultrathin Ti layer was necessary for the adhesion of Pt on TiN. The other half was subjected to the same fabrication steps with the addition of a 2 nm Al layer between the HZO and the top electrode TiN. The exact sputtering parameters could be found in the work by Bouaziz et al.[23] Both resulting samples were annealed in a tubular furnace at 450 °C under N_2 atmosphere for 30 min.

Device Characterization: The thicknesses of the layers were verified by X-ray reflectometry (XRR) and structural properties were measured by GI-XRD with a Rigaku Smartlab diffractometer.

Electrical characterization was carried out using a Keithley 4200-SCS Semiconductor Parameter Analyzer Characterization System equipped with SMUs, RPMs, and CVUs. Voltage was applied through the bottom electrode by contacting a dielectrically broken-down device and the top electrode of the device of interest. For the study of the impact of pulse width and height, the cycling pulses were square shaped with 500 ns ramps and 10 μs pauses at 0 V between them. The duration was varied first, from 1 to 500 μs with the height maintained at 4 V. The voltage was then increased from 3 to 4.75 V with a pulse width fixed at 20 μs. Each pulse form was applied once to one device until breakdown. Two reading protocols were used during cycling: a PUND sequence to measure polarization followed by two low voltage pulses to read the current value with a programming pulse in between to switch polarization state. The PUND pulses were triangular with ramps of 20 μs and maximum voltage equal to cycling voltage. Read pulses were 1 V high and 5 ms long with 500 ns ramps. The devices were 100 μm in diameter. The exact setup for electrical characterization was also described by Bouaziz et al.[23]

Acknowledgements

This work was undertaken on the NanoLyon technology platform and received funding from the European Union's Horizon 2020 research and innovation programme under Grant Agreement no. 780302 (3eFERRO), under the Marie Sklodowska-Curie Grant Agreement no. 801512 (i3E ECLAUSion), and French Public Authorities through the NANO2022 program.

Conflict of Interest

The authors declare no conflict of interest.

© 2022 Wiley-VCH GmbH

Data Availability Statement

The data that support the findings of this study are available from the corresponding author upon reasonable request

Keywords

aluminum, ferroelectric HZO, ferroelectric tunnel junction, thin films

Received: November 16, 2021
Revised: March 7, 2022
Published online:

[1] R. Khosla, S. K. Sharma, *ACS Appl. Electron. Mater.* **2021**, acsaelm.0c00851.
[2] T. S. Böscke, J. Müller, D. Bräuhaus, U. Schröder, U. Böttger, *Appl. Phys. Lett.* **2011**, *99*, 102903.
[3] M. H. Park, T. Schenk, U. Schroeder, in *Ferroelectricity in Doped Hafnium Oxide: Materials, Properties and Devices* (Eds.: U. Schroeder, C. S. Hwang, H. Funakubo), Woodhead Publishing Series in Electronic and Optical Materials, Woodhead Publishing, Duxford **2019**, pp. 49–74.
[4] M. Dragoman, M. Aldrigo, D. Dragoman, S. Iordanescu, A. Dinescu, M. Modreanu, *IEEE Nanotechnol. Mag.* **2021**, *15*, 8.
[5] T. Onaya, T. Nabatame, N. Sawamoto, A. Ohi, N. Ikeda, T. Nagata, A. Ogura, *Microelectron. Eng.* **2019**.
[6] S. S. Cheema, N. Shanker, C.-H. Hsu, A. Datar, J. Bae, D. Kwon, S. Salahuddin, arXiv:2007.06182 [cond-mat, physics:physics], **2020**.
[7] S. Oh, H. Kim, A. Kashir, H. Hwang, *Appl. Phys. Lett.* **2020**, *117*, 252906.
[8] R. Meyer, J. R. Contreras, A. Petraru, H. Kohlstedt, *Integr. Ferroelectr.* **2004**, *64*, 77.
[9] B. Max, M. Hoffmann, S. Slesazeck, T. Mikolajick, **2018**, 142–145.
[10] A. Shekhawat, G. Walters, N. Yang, J. Guo, T. Nishida, S. Moghaddam, *Nanotechnology* **2020**, *31*, 39LT01.
[11] H. Ryu, H. Wu, F. Rao, W. Zhu, *Sci. Rep.* **2019**, *9*, 20383.
[12] J. Hwang, Y. Goh, S. Jeon, *IEEE Trans. Electron Devices* **2021**, *68*, 841.
[13] M. Materano, P. D. Lomenzo, A. Kersch, M. H. Park, T. Mikolajick, U. Schroeder, *Inorg. Chem. Front.* **2021**, *8*, 2650.
[14] F. Ambriz-Vargas, G. Kolhatkar, R. Thomas, R. Nouar, A. Sarkissian, C. Gomez-Yáñez, M. A. Gauthier, A. Ruediger, *Appl. Phys. Lett.* **2017**, *110*, 093106.
[15] S. J. Kim, D. Narayan, J.-G. Lee, J. Mohan, J. S. Lee, J. Lee, H. S. Kim, Y.-C. Byun, A. T. Lucero, C. D. Young, S. R. Summerfelt, T. San, L. Colombo, J. Kim, *Appl. Phys. Lett.* **2017**, *111*, 242901.
[16] T. Shiraishi, K. Katayama, T. Yokouchi, T. Shimizu, T. Oikawa, O. Sakata, H. Uchida, Y. Imai, T. Kiguchi, T. J. Konno, H. Funakubo, *Appl. Phys. Lett.* **2016**, *108*, 262904.
[17] G. D. Wilk, R. M. Wallace, J. M. Anthony, *J. Appl. Phys.* **2001**, *89*, 5243.
[18] K. M. Rabe, M. Dawber, C. Lichtensteiger, C. H. Ahn, J.-M. Triscone, in *Physics of Ferroelectrics: A Modern Perspective, Topics in Applied Physics*, Springer, Berlin, Heidelberg **2007**, pp. 1–30.
[19] M. H. Park, D. H. Lee, K. Yang, J.-Y. Park, G. T. Yu, H. W. Park, M. Materano, T. Mittmann, P. D. Lomenzo, T. Mikolajick, U. Schroeder, C. S. Hwang, *J. Mater. Chem. C* **2020**, *8*, 10526.
[20] D. R. Islamov, V. A. Gritsenko, T. V. Perevalov, V. A. Pustovarov, O. M. Orlov, A. G. Chernikova, A. M. Markeev, S. Slesazeck, U. Schroeder, T. Mikolajick, G. Y. Krasnikov, *Acta Mater.* **2019**, *166*, 47.
[21] D. R. Islamov, A. G. Chernikova, M. G. Kozodaev, A. M. Markeev, T. V. Perevalov, V. A. Gritsenko, O. M. Orlov, *J. Phys.: Conf. Ser.* **2017**, *864*, 012002.
[22] D. B. Strukov, G. S. Snider, D. R. Stewart, R. Stanley Williams, *Nat. Lett.* **2008**.
[23] J. Bouaziz, P. Rojo Romeo, N. Baboux, R. Negrea, L. Pintilie, B. Vilquin, *APL Mater.* **2019**.

UNCORRECTED PROOF

© 2022 Wiley-VCH GmbH

physica status solidi pss rrl
rapid research letters

Please complete this form and return it via E-Mail to the Editorial Office.
E-mail: pss.rapid@wiley-vch.de

By providing the payment information below, you agree that you are responsible for the charges and taxes (as applicable), and that you will promptly pay the invoice in accordance with the terms thereof.

Reprint Order Form

Manuscript No.: ______________________________
Customer No.: (if available) ______________________
Purchase Order No.: ______________________
Author: ______________________________

Charges for Reprints in Euro (excl. VAT), prices are subject to change. Minimum order 50 copies

No. of pages	50 copies	100 copies	150 copies	200 copies	300 copies	500 copies
1– 4	345,—	395,—	425,—	445,—	548,—	752,—
5– 8	490,—	573,—	608,—	636,—	784,—	1077,—
9–12	640,—	739,—	786,—	824,—	1016,—	1396,—
13–16	780,—	900,—	958,—	1004,—	1237,—	1701,—
17–20	930,—	1070,—	1138,—	1196,—	1489,—	2022,—
every additional 4 pages	147,—	169,—	175,—	188,—	231,—	315,—

Information regarding VAT: The charges for publication of *cover pictures /reprints/issues/poster/Video abstracts/* are considered to be "supply of services" and therefore subject to German VAT. However, if you are an institutional customer outside Germany, the tax can be waived if you provide us with the valid VAT number of your company. Non-EU customers may have a VAT number starting with "EU" instead of their country code, if they are registered with the EU tax authorities. If you do not have a valid EU VAT number and you are a taxable person doing business in a non-EU country, please provide a certification from your local tax authorities confirming that you are a taxable person under local tax law. Please note that the certification must confirm that you are a taxable person and are conducting an economic activity in your country. **Note:** certifications confirming that you are a tax-exempt legal body (non-profit organization, public body, school, political party, etc.) in your country do not exempt you from paying German VAT.

Please send me send bill me for

☐ no. of reprints

☐ high-resolution PDF file (330 Euro excl. VAT)
E-mail address: ________________

❖ Special Offer:
If you order 200 or more reprints you will get a PDF file for half price.

Please note: It is not permitted to present the PDF file on the internet or on company homepages.

Cover Posters (prices excl. VAT)
Posters of published covers are available in two sizes:

☐ DIN A2 42 x 60 cm / 17 x 24in (one copy: 39 Euro)

☐ DIN A1 60 x 84 cm / 24 x 33in (one copy: 49 Euro)

Postage for shipping (prices excl. VAT)
overseas +25 Euro
within Europe +15 Euro

VAT number: ________________________

Mail reprints / copies of the issue to:

____
____
____
____
____

Send bill to:

____
____
____
____

☐ **I will pay by bank transfer**

☐ **I will pay by credit card**

VISA, Mastercard and AMERICAN EXPRESS
For your security please use this link (Credit Card Token Generator) to create a secure code Credit Card Token and include this number in the form instead of the credit card data. Click here:
https://www.wiley-vch.de/editorial_production/index.php

CREDIT CARD TOKEN NUMBER

						V									

____
Date, Signature

Wiley-VCH GmbH– A company of John Wiley & Sons, Inc. -
Location of the Company: Weinheim - Trade Register: Mannheim, HRB 736569
Managing Directors: Sabine Haag und Guido Herrmann

WILEY-VCH